Journal of Photochemistry and Photobiology A: Chemistry 223 (2011) 202–211

Contents lists available at SciVerse ScienceDirect

Journal of Photochemistry and Photobiology A: Chemistry

journal homepage: www.elsevier.com/locate/jphotochem

Determination of kinetic constants of a photocatalytic reaction in micro-channel reactors in the presence of mass-transfer limitation and axial dispersion

Guillaume Charles, Thibault Roques-Carmes*, Nidhal Becheikh, Laurent Falk, Jean-Marc Commenge, Serge Corbel

Laboratoire Réactions et Génie des Procédés, UPR 3349 CNRS, Nancy-Université 1, rue Grandville, BP 20451, 54001 Nancy Cedex, France

ARTICLE INFO

Article history:
Received 5 April 2011
Received in revised form 19 August 2011
Accepted 26 August 2011
Available online 6 September 2011

Keywords:
Micro-channel reactor
Photocatalysis
Titanium dioxide
Kinetic constants
Mass-transfer
Stereolithography

ABSTRACT

The main objective of this article is to evaluate quantitatively the kinetic constants of a photocatalytic reaction in micro-channel reactors despite the presence of a radial concentration profile (mass-transfer limitation) and axial dispersion. Photocatalytic micro-channel reactors with immobilized titanium dioxide as photocatalyst have been fabricated using stereolithography process. The photocatalytic degradation of salicylic acid is investigated as a function of rectangular micro-channel size, contaminant concentration, flow rate and incident UV light intensity. All the micro-channel reactors exhibit the same tendency. Higher degradation is observed for high incident light intensities, low pollutant concentrations and flow rates. A simple equation for the determination of the kinetic constants during the photocatalytic degradation is reported. The equation includes the hydrodynamic properties and a surface reaction model for the photocatalytic reaction (monomolecular Langmuir–Hinshelwood kinetics). In the experimental system, we demonstrate that some external mass-transfer limitation and axial dispersion occur. They are included in the modeling with calculated values of the mass-transfer coefficient of salicylic acid from the solution to the catalyst surface and the axial dispersion coefficient. A single couple of values of the reaction rate constant k and the adsorption equilibrium constant K represent properly the experimental degradation ratios for all reactor dimensions, flow rates and pollutant concentrations. The major parameter that controls the values of the reaction rate constant is the incident light intensity. The dependence of the reaction rate on the incident light intensity is first order.

1. Introduction

Photocatalysis is a potential technology for the destruction of organic contaminants in water, such as aromatic compounds, which present a potential hazard to the environment [1–3]. The mineralization of remaining traces of organic contaminants in water together with the removal of microorganisms make photocatalysis a very suitable technique for the treatment of wastewater but also a valuable alternative to conventional drinking water treatment and for the production of ultrapure water for pharmaceutical applications [4].

Titanium dioxide (TiO_2) is the most commonly used semiconductor photocatalyst since it is highly photoactive, photostable, biologically and chemically inert, and relatively inexpensive. The photochemical technology using TiO_2 photocatalyst for the water treatment process is known as a clean method. Regarding economical and practical reasons, it has become clear that the most useful form of TiO_2 photocatalyst is that of a film or coating on a convenient support [5,6]. However, immobilized systems have the problem that they are difficult to scale-up, have low interfacial surface areas and mass-transfer limitations may occur [7,8].

To predict the performance of a photocatalytic reactor with immobilized catalyst, it is necessary to previously determine the intrinsic kinetic reaction rate constants. That contributes significantly to shortening the delays from laboratory development to industrial scale-up. An important consideration during kinetic constant determination is the use of a reactor operating in a regime in which mass-transfer limitations are not predominant [7,9]. The kinetic parameters are then independent of the reactor configuration. This can be achieved by using a well-mixed batch reactor [10] or micro-reactors [11,12]. However, micro-reactors have only very recently been investigated for the determination of the kinetic constants of photocatalytic reactions [11–15]. For photochemical reactions in particular, micro-reactors exhibit higher spatial illumination homogeneity and better light penetration through the entire reactor depth in comparison to large-scale reactors [13]. Besides the miniaturization of the reaction system itself, light emitting sources

* Corresponding author. Tel.: +33 03 83 37 50 89; fax: +33 03 83 37 81 20.
E-mail address: thibault.roques-carmes@ensic.inpl-nancy.fr (T. Roques-Carmes).

1010-6030/$ – see front matter © 2011 Elsevier B.V. All rights reserved.
doi:10.1016/j.jphotochem.2011.08.019

on the micro or even nanoscale near the catalyst are necessary to achieve uniform and maximized illumination [16]. For instance, Gorges et al. [11] used an array of 11 UV-A LEDs mounted on a printed circuit board to uniformly illuminate 19 micro-channels with a cross-section of approximately 300 μm × 200 μm.

However, to avoid the difficult fabrication of micro or nanoreactors and the prohibitive cost of the light sources on the micro or nanoscale, we propose to introduce micro-channel reactors with typical characteristic dimensions between 500 μm and 2 mm. The size of the channel is more adapted to future industrial implementation. Unfortunately, this particular configuration may lead to axial and radial concentration profiles (mass-transfer limitation) under laminar flow. To this extent, it becomes then necessary to apply a computational fluid dynamics (CFD) approach to determine the kinetic parameters [17–20]. One of the aims of this article is to describe a simple and rapid methodology for the accurate determination of the kinetic constants in the presence of mass-transfer limitation and axial dispersion assuming that all photocatalytic users do not have access to CFD tools.

In this paper, photocatalytic rectangular micro-channel reactors with immobilized titanium dioxide as photocatalyst are designed, constructed and tested. The micro-channel reactors are fabricated using stereolithography process which allows the fabrication of complex forms with a great flexibility [21,22]. This study focuses on the photocatalytic degradation of a model component, salicylic acid, because it is easily degraded. The rectangular micro-channel size, contaminant concentration, flow rate and incident UV light intensity are varied. An equation for the determination of the kinetic constants is developed. The model takes into account the hydrodynamic properties and the photocatalytic surface reaction. The generic nature of the model means that it can be applied for the determination of the kinetic constants, in the presence of mass-transfer limitation, for any reactor design and any organic pollutant regardless of the photocatalyst nature if the reaction rate can be modeled by a Langmuir–Hinshelwood law.

2. Materials and methods

2.1. Fabrication of photocatalytic micro-channel reactors

The rectangular micro-channel reactors were fabricated in epoxy resin by a home-made stereolithography apparatus using a UV Nd–YAG laser [21–24]. The stereolithography technique is based on the process of photopolymerisation, in which a liquid resin is converted to a solid polymer on exposure to laser radiation. The models are produced by curing successive layers of resin material until a three-dimensional object is formed. Fig. 1a depicts a photographic view of the polymeric micro-reactor. The titanium dioxide samples were deposited on the micro-channel reactor (inner surface of the channel) according to the procedure of Furman et al. [21]. An aqueous suspension of TiO_2 Degussa P25 (Evonik) of 4 g L^{-1} at pH 3 was poured on the channel and the excess removed. The wetted channel was dried at 50 °C for 1 h. This coating process was repeated 20 times. After rinsing under running distilled water in order to remove loose particles, the amount of deposit was determined by weighing the dried reactor before and after the deposition. This resulted in a coating thickness of 5 ± 1 μm (determined by profilometry) and a surface load of 2.8 ± 0.3 mg/cm^2, this value being above the minimal load generally required for complete light absorption [3,25]. This experimental procedure enabled to control the mass of the coated catalyst and to obtain a uniform layer on the entire surface of the channel. Note that only the two side walls and the bottom of the channel were covered with the photocatalyst. Following the deposition of the catalyst, the micro-reactor was sealed with a glass top plate using an epoxy glue.

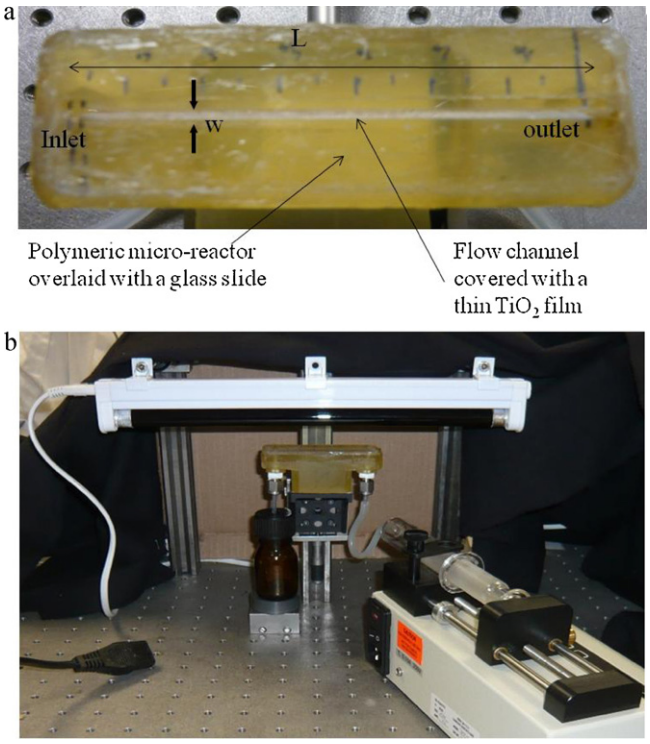

Fig. 1. (a) Photographic view of the micro-channel reactor. (b) Experimental setup for photocatalytic reactions with a micro-channel reactor.

The total catalyst surface A_{cat} is obtained using:

$$A_{cat} = L(w + 2h) \quad (1)$$

where L denotes the channel length, w the channel width and h the channel height.

Ray and Beenackers [7] identified the illuminated specific surface area (κ) of a photocatalyst within the reactor that is in contact with the reaction liquid as an important design parameter for the construction of photocatalytic reactors. κ is calculated using the following formula:

$$\kappa = \frac{2h + w}{wh} \quad (2)$$

The characteristics of the three rectangular micro-channel reactors with different dimensions are shown in Table 1. It appears that the κ values for our micro-channel reactors surpass the values for other macro-reactor types due to the large surface-to-volume ratio inherent to any micro-structured reactor [13]. Then, from the geometrical estimation, we conclude that the photocatalytic reaction takes place mainly at the inner surface of the channel.

2.2. Photocatalytic reaction system

The experimental setup used for the photocatalytic tests is shown in Fig. 1b. An aqueous solution of salicylic acid was introduced into the micro-channel reactor with a syringe

Table 1
Geometrical characteristics of the rectangular micro-channel reactors. w refers to the channel width, h to the channel height, L to the channel length, κ to the specific catalyst surface area per volume unit of liquid treated inside the reactor and A_{cat} to the total catalyst surface.

	Width, w (mm)	Height, h (mm)	Length, L (mm)	κ (m^{-1})	A_{cat} (mm^2)
R1	1	0.5	70	4000	140
R1.5	1.5	0.5	70	3333	175
R2	2	0.5	70	3000	210

pump (KdScientific, KDS-100-Ce). The flow regime inside the micro-reactor channels was laminar since the Reynolds numbers (Re = 0.8–7.0) were smaller than the critical Re. A flexible tube at the outlet of the reactor enabled to collect the irradiated solution samples. The micro-channel reactors operated under continuous flow operation (permanent regime) as plug-flow reactor.

A UV fluorescent lamp (Oaric Halolite, light power 8 W) was positioned outside the reactor (Fig. 1b). It was located at 1 cm above the reactor and parallel to the central axis of the channel. The incident light power was recorded by an ultraviolet radiometer and indicated a spectral response centered at 365 nm with a half bandwidth of 12 nm. The incident light energy density at the surface of the catalyst was $I_{incident}$ = 1.5 mW/cm^2 unless stated otherwise. The incident light energy density at the surface of the catalyst could be varied by changing the distance between the reactor and the lamp.

To characterize the photocatalytic performance of the micro-channel reactors, the degradation of salicylic acid, a widely employed compound for the testing of photocatalytic systems, was investigated [24,25]. The photocatalytic process was followed by monitoring the disappearance of salicylic acid. Solutions of salicylic acid were prepared with Milli-Q water and aerated before use. The photocatalytic experiments were performed at pH 6. At the start of every experiment, introduction of the reactant into the system was performed under light irradiation. Before samples were taken, the solution was passed through the reactor for at least 1 h to ensure that adsorption equilibrium and steady-state conditions had been reached. The salicylic acid concentration after photoreaction (C_{out}) was measured by HPLC. The HPLC system was equipped with a variable Shimadzu SPD-20A UV-Vis detector, a Rheodyne Model 7725 injector, a loop size of 20 μL and a Shimadzu LC-20AT pump. Chromatograms were registered with standard reversed-phase HPLC using a Lichrosorb RP-18 column (250 mm × 4.6 mm, i.e. particle size 5 μm, Supelco-Inc). The eluent was a mixture of 70% (v/v) methanol and 30% (v/v) water containing 0.1% (v/v) of phosphoric acid. The flow rate was 1 mL min^{-1} and the detection wavelength was 295 nm.

The experimental degradation ratio of salicylic acid during its contact with the catalyst is defined by:

$$X = \frac{C_{in} - C_{out}}{C_{in}} \quad (3)$$

where C_{in} and C_{out} denote the salicylic acid concentrations at the inlet and the outlet of the reactor, respectively.

Prior to the photocatalytic experiment, the experimental system was operated for several hours using distilled water to remove any organic and inorganic impurities adsorbed on the surface of the catalyst as well as any TiO_2 coating particles that were not strongly attached to the surface of the micro-channel reactor.

2.3. Residence time distribution

In order to characterize the flow in the micro-channel reactors, the liquid residence time distribution (RTD) was determined. The following setup (Fig. 2) was used to evaluate the RTD in the reactors. The reactor R2 used for RTD measurements had an internal volume of 70 μL which was smaller than the volume of the overall measuring unit. This meant that the residence time response of an inert tracer was strongly influenced by the measuring setup itself. For this reason, the flow characteristics in the micro-channel reactor were isolated from measurements of the concentration of a tracer at the inlet and at the outlet of the reactor. As inert passive tracer, nigrosin was used since it had strong UV-light absorption with an absorption maximum at approximately 300 nm. Due to the linear response and very short response times of the UV-sensor, the acquired signals could then be easily treated in order to access the concentration signals as a function of time [26,27]. Prior to each experiment, the reactor was rinsed with water using a syringe pump (KdScientific, KDS-100-Ce). Switching a valve then allowed the introduction of an aqueous solution of nigrosin (0.2 g L^{-1}) by a continuous switch of the feed pump at a given flow rate. The acquisition system was then activated and the luminous intensities were recorded as a function of time. In our configuration, it was necessary to obtain the shape of the entering signal before the reactor $E_{inlet}(t)$ and the shape of the output signal at the outlet of the reactor $E_{outlet}(t)$. For this purpose, the signal was measured without the reactor ($E_{inlet}(t)$) and later with the micro-channel reactor ($E_{outlet}(t)$). Normalization of these signals then allowed the RTD of the liquid in the micro-channel reactor volume to be studied.

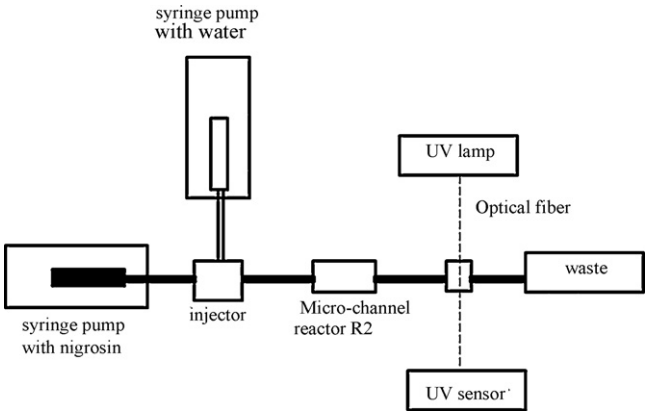

Fig. 2. Schematic of the experimental apparatus for residence time distribution measurements.

Calculation of the first-order moment of both the inlet $\left(\overline{t_{s,inlet}}\right)$ and the outlet $\left(\overline{t_{s,outlet}}\right)$ signals provided the mean residence time in the reactor $\overline{t_{s,R}}$:

$$\overline{t_{s,R}} = \overline{t_{s,outlet}} - \overline{t_{s,inlet}} \quad (4)$$

Estimation of the second-order moment of both the inlet ($\mu_{2,inlet}$) and the outlet ($\mu_{2,outlet}$) signals gave the variance σ_R^2:

$$\sigma_R^2 = \sigma_{outlet}^2 - \sigma_{inlet}^2 = \left(\mu_{2,outlet} - \left(\overline{t_{s,outlet}}\right)^2\right) - \left(\mu_{2,inlet} - \left(\overline{t_{s,inlet}}\right)^2\right) \quad (5)$$

The mean residence time and the variance are related to the experimental reactor Peclet number Pe_R [28], as:

$$Pe_R = 2\frac{\left(\overline{t_{s,R}}\right)^2}{\sigma_R^2} \quad (6)$$

3. Determination of the kinetic constants

3.1. Langmuir–Hinshelwood model

The photocatalytic degradation of salicylic acid is often described to be governed by Langmuir–Hinshelwood kinetics [3,25]. The model assumes (a) low concentration of the intermediate products, (b) similar binding characteristics on TiO_2 of the intermediate products and the parent compound, (c) non-competitive adsorption for the same active sites on TiO_2 between the organic contaminant and the solvent and (d) much slower attack of the adsorbed pollutant molecule by a surface reactive species (OH radical, hole) than the rate of disappearance of the reactive species.

The equation for reaction rate takes the form of the following equation [29]:

$$r = \frac{kKC_s}{1+KC_s} \tag{7}$$

where r denotes the reaction rate of salicylic acid degradation, C_s the concentration of salicylic acid at the surface of the catalyst, k the reaction rate constant and K the adsorption equilibrium constant. The reaction rate constant k depends on the light intensity absorbed by the catalyst but not on the catalyst load under our experimental conditions. The adsorption equilibrium constant K is affected by the temperature and the affinity between the pollutant and the catalyst.

Assuming a steady-state approximation, the mass flux towards the surface of the catalyst is equal to the chemical consumption in salicylic acid at the support surface (Langmuir–Hinshelwood rate):

$$r = k_{m,ext}(C - C_s) = \frac{kKC_s}{1+KC_s} \tag{8}$$

where C is the pollutant concentration of the liquid flow and $k_{m,ext}$ is the mass-transfer coefficient.

The solution of Eq. (8) gives the expression for C_s:

$$C_s = \frac{-k_{m,ext} + k_{m,ext}KC - kK + \sqrt{(-k_{m,ext} + k_{m,ext}KC - kK)^2 + 4k_{m,ext}^2 KC}}{2k_{m,ext}K} \tag{9}$$

C_s depends on the chemical consumption (kinetic constant k and adsorption constant K) which acts as a "sink" and on the external mass-transfer (mass-transfer coefficient $k_{m,ext}$, flow rate and concentration C) [30]. When the external mass-transfer is efficient enough, C_s tends to be equal to C and the degradation rate only depends on the chemical kinetics (see Section 3.2). In the case of a high chemical consumption compared to the mass-transfer process, an important concentration gradient takes place in the boundary layer and the concentration C_s can become lower than the concentration in the liquid flow C (see Section 3.3). Therefore, the degradation rate becomes lower, which reduces the efficiency of the photocatalyst. This is true in particular for low flow rates.

3.2. Perfect plug-flow reactor

The reactor is considered to be a perfect plug-flow reactor. We also assume the absence of limitation by mass-transfer (kinetic regime), i.e. C_s tends to be equal to C and the degradation rate only depends on the kinetics.

The mass balance on a small volume of support for a plug-flow reactor is:

$$QdC = -\frac{kKC}{1+KC}dV \tag{10}$$

Integrating Eq. (10) between the reactor inlet and outlet yields:

$$\frac{1}{kK}\ln\left(\frac{C_{out}}{C_{in}}\right) + \frac{1}{k}(C_{out} - C_{in}) = -\frac{V}{Q} \tag{11}$$

with V the volume of the reactor, Q the flow rate, C_{in} and C_{out} the inlet and outlet concentrations, respectively. We introduce the degradation ratio $X = 1 - C_{out}/C_{in}$. It will be shown experimentally that the kinetic constant k and the equilibrium constant K are apparent constants. For that reason, we consider that $k = k_{app}$ and $K = K_{app}$. Eq. (11) can be written as:

$$-\frac{V}{QC_{in}X} = \frac{1}{k_{app}K_{app}}\frac{\ln(1-X)}{C_{in}X} - \frac{1}{k_{app}} \tag{12}$$

A plot of $-V/(QC_{in}X)$ versus $\ln(1-X)/C_{in}X$ should be linear and allow the determination of the two constants k_{app} and K_{app}.

3.3. Plug-flow reactor in the presence of a radial concentration profile and axial dispersion

The mass balance through a plug-flow reactor in the presence of a radial concentration profile (mass-transfer limitation) and axial dispersion is given by:

$$\frac{d^2C}{dx^2} - \frac{u}{D_a}\frac{dC}{dx} - \frac{1}{D_a}k_{m,ext}(C - C_s) = 0 \tag{13}$$

with u being the axial mean velocity in the micro-channel reactor, D_a the axial dispersion coefficient and x the axial coordinate.

However, the analytical solution of Eq. (13) using the expression of C_s (Eq. (9)) is not analytically convenient. In order to overcome this issue, a simplification is proposed. The relation between the concentrations C and C_s can be obtained by rewriting Eq. (8) as:

$$C = C_s + \frac{1}{k_{m,ext}}\frac{kKC_s}{(1+KC_s)} \approx C_s\left(1 + \frac{kK}{k_{m,ext}(1+KC_{si})}\right) = A^{-1} \times C_s \tag{14}$$

with

$$A = \left(1 + \frac{kK}{k_{m,ext}(1+KC_{si})}\right)^{-1} = \frac{k_{m,ext}(1+KC_{si})}{k_{m,ext}(1+KC_{si}) + kK} \tag{15}$$

It is then considered that C_{si} is a constant concentration.

Substituting Eq. (14) into Eq. (13) yields:

$$\frac{d^2C}{dx^2} - \frac{u}{D_a}\frac{dC}{dx} - \frac{1}{D_a}k_{m,ext}C(1-A) = 0 \tag{16}$$

The solution of Eq. (16) can be written as:

$$C = C_{in}\ \exp\left(\frac{x}{2}\left(\frac{u}{D_a} - \sqrt{\left(\frac{u}{D_a}\right)^2 + \frac{4k_{m,ext}(1-A)}{D_a}}\right)\right) \tag{17}$$

or

$$C = C_{in}\ \exp\left(\frac{x}{2}\left(\frac{u}{D_a} - \sqrt{\left(\frac{u}{D_a}\right)^2 + 4\frac{1}{D_a}\frac{kKk_{m,ext}}{k_{m,ext}(1+KC_{si}) + kK}}\right)\right) \tag{18}$$

The outlet concentration C_{out} can be calculated using $x = L$:

$$C_{out} = C_{in}\ \exp\left(\frac{L}{2}\left(\frac{u}{D_a} - \sqrt{\left(\frac{u}{D_a}\right)^2 + \frac{4k_{m,ext}(1-A)}{D_a}}\right)\right) \tag{19}$$

The degradation ratio of salicylic acid during its contact with the catalyst is defined by:

$$X = 1 - \frac{C_{out}}{C_{in}} = 1 - \exp\left(\frac{L}{2}\left(\frac{u}{D_a} - \sqrt{\left(\frac{u}{D_a}\right)^2 + 4\frac{1}{D_a}\frac{kKk_{m,ext}}{k_{m,ext}(1+KC_{si}) + kK}}\right)\right) \tag{20}$$

Eq. (20) constitutes our central result. It is first necessary to calculate u, D_a, $k_{m,ext}$, and C_{si}. The axial mean velocity u is estimated as the ratio of the flow rate Q to the channel cross-section Ω ($\Omega = w \times h$), i.e. $u = Q/\Omega$.

In laminar flow, the axial dispersion coefficient D_a is given by

$$D_a = D + \frac{u^2 d_h^2}{192D} \tag{21}$$

where D is the molecular diffusion coefficient and d_h is the hydrodynamic diameter of the micro-channel. The value of D for salicylic acid is 0.98×10^{-9} m^2 s^{-1} [31,32].

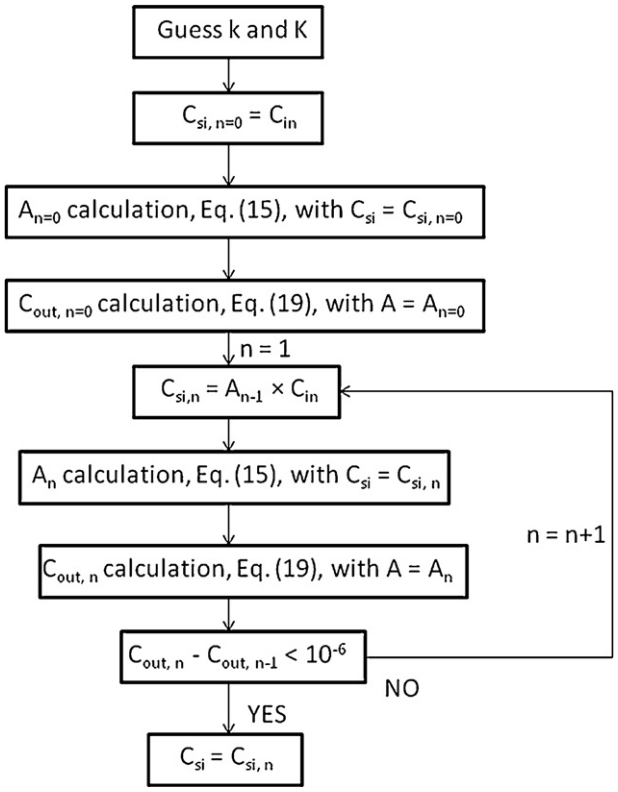

Fig. 3. Method used for the calculation of C_{si}.

The mass-transfer coefficient $k_{m,ext}$ can be estimated from Sherwood number using

$$\mathrm{Sh} = \frac{k_{m,ext} d_h}{D} \tag{22}$$

Barlay Ergu et al. [33] investigated experimentally mass-transfer in a rectangular micro-channel having a width of 3.7 mm, height of 0.1 mm and length of 35 mm by using the electrochemical limiting diffusion current technique. They reported a correlation of the form:

$$\mathrm{Sh} = 2.076 \times \mathrm{Re}^{0.28} \left(\frac{L}{d_h}\right)^{-0.12} \times \mathrm{Sc}^{1/3} \tag{23}$$

where Re is the Reynolds number, Sc the Schmidt number and L the micro-channel length (70 mm). The Schmidt number is calculated using $\mathrm{Sc} = \mu/\rho D$, with μ and ρ the viscosity and the density of the solution, respectively.

An iterative methodology is used to determine C_{si}. The termination criterion is to obtain a constant value of C_{out}. The calculation scheme is described in Fig. 3.

In Eq. (20), two parameters are a priori unknown, namely k and K. To fit the experimental data to the model we use the following calculation scheme. Initially, we guess the values of k and K. For these values, the numerical solution of Eq. (20) is calculated. The resulting curve is then compared to the experimental degradation ratio as a function of the flow rate. The values of k and K are modified in such a way that the distance between the numerical solution and the experiment is minimal.

4. Results and discussion

The complete photocatalytic degradation of salicylic acid can be summarized as:

$$C_7H_6O_3 + 7O_2 \xrightarrow{h\nu,\,TiO_2} 7CO_2 + 3H_2O$$

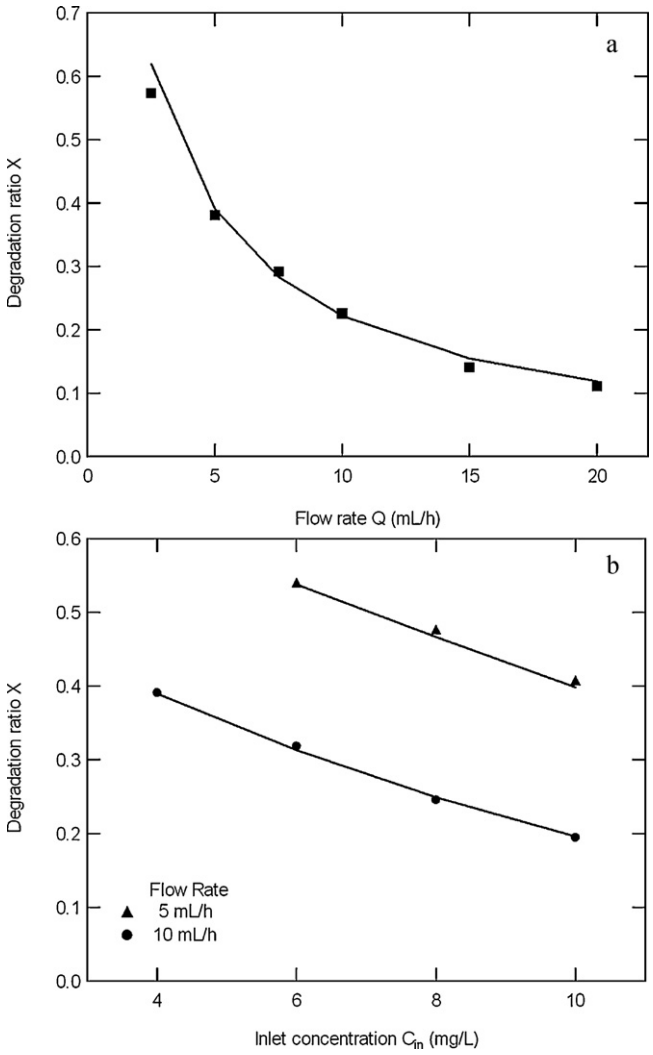

Fig. 4. Degradation of salicylic acid in R1 as a function of (a) the flow rate with $C_{in} = 10$ mg/L and $I_{incident} = 1.5$ mW/cm^2. The solid line is the best fit, calculated with Eq. (20). Fitting parameters: $k = 2.06 \times 10^{-3}$ mmol L^{-1} s^{-1} and $K = 23$ L mmol^{-1}. (b) The inlet salicylic acid concentration at different flow rates with $I_{incident} = 1.5$ mW/cm^2. The points are experimental data, the lines are model results calculated using Eq. (20) and the fitting parameters k and K. Geometrical characteristics of R1: $w = 1$ mm, $h = 0.5$ mm and $L = 70$ mm.

Guinea et al. [34] described 2,3-dihydroxybenzoic acid, 2,6-dihydroxybenzoic acid and maleic acid to be the major intermediates for the photocatalytic degradation of salicylic acid. However, in our experiments with the micro-channel reactors, we could not detect any of these substances with the employed HPLC method.

Figs. 4–6 show the influence of the flow rate, inlet concentration and incident light intensity on the degradation ratio of salicylic acid in the reactors R1, R1.5 and R2, respectively. The photocatalytic activity of the micro-channel reactors is confirmed from the degradation of salicylic acid. These results clearly indicate the successful integration of the photoreactive TiO_2 into the micro-channel systems. All the reactors show the same trend. Higher degradation is observed for lower inlet concentrations. Furthermore, the degradation decreases with the flow rate, which can be explained by the reduction of the residence time of the reactants in the micro-channels. The degradation performance is also affected by the incident light intensity (Fig. 5a). The increase of the incident UV light intensity results in an enhancement of the degradation.

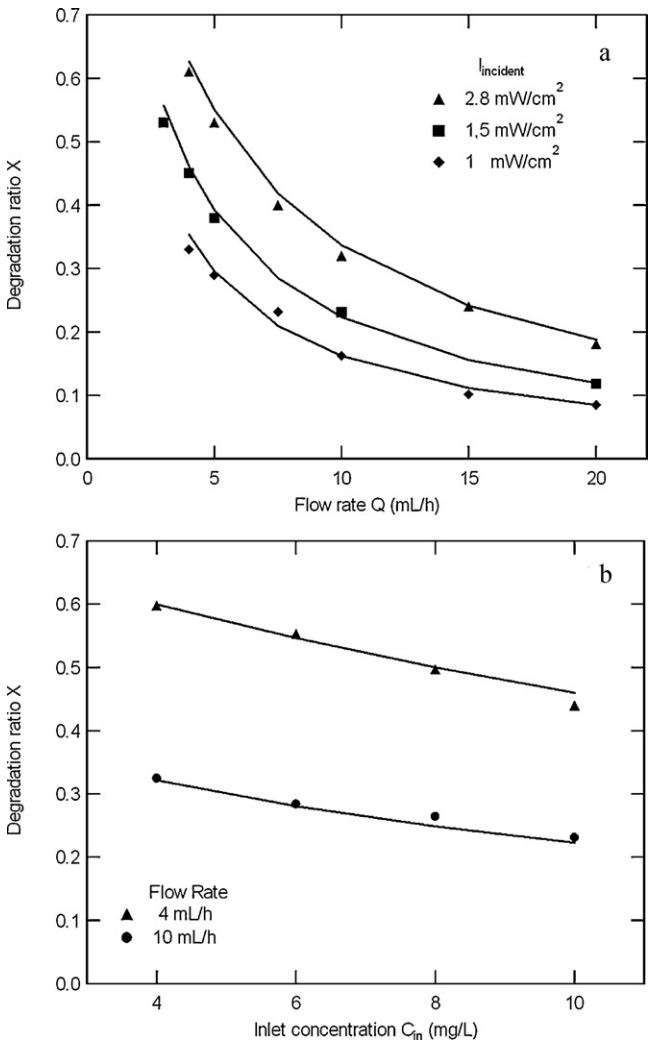

Fig. 5. Degradation of salicylic acid in R1.5 as a function of (a) the flow rate at different incident light intensities ($I_{incident}$) with C_{in} = 10 mg/L. The solid lines are the best fit, calculated with Eq. (20). Fitting parameters: $k = 2.92 \times 10^{-3}$ mmol L^{-1} s^{-1} and K = 25 L mmol^{-1} for $I_{incident}$ = 2.8 mW/cm^2; $k = 1.68 \times 10^{-3}$ mmol L^{-1} s^{-1} and K = 25 L mmol^{-1} for $I_{incident}$ = 1.5 mW/cm^2; $k = 1.11 \times 10^{-3}$ mmol L^{-1} s^{-1} and K = 25 L mmol^{-1} for $I_{incident}$ = 1 mW/cm^2. (b) The inlet salicylic acid concentration at different flow rates with $I_{incident}$ = 1.5 mW/cm^2. The points are experimental data, the lines are model results calculated using Eq. (20) and the fitting parameters k and K. Geometrical characteristics of R1.5: w = 1.5 mm, h = 0.5 mm and L = 70 mm.

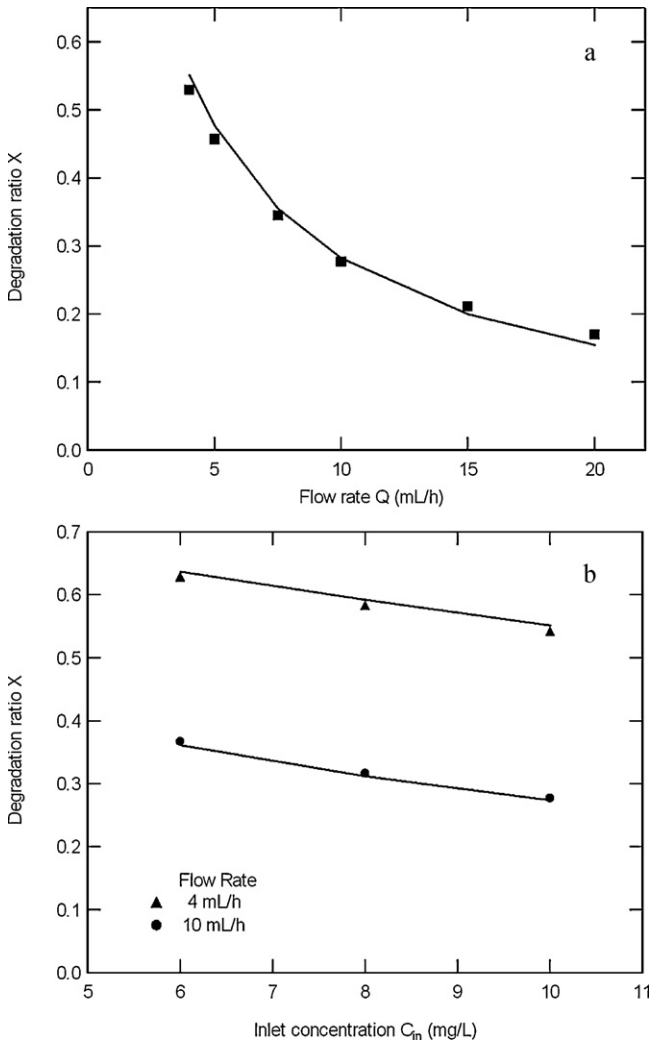

Fig. 6. Degradation of salicylic acid in R2 as a function of (a) the flow rate with C_{in} = 10 mg/L and $I_{incident}$ = 1.5 mW/cm^2. The solid line is the best fit, calculated with Eq. (20). Fitting parameters: $k = 1.70 \times 10^{-3}$ mmol L^{-1} s^{-1} and K = 24 L mmol^{-1}. (b) The inlet salicylic acid concentration at different flow rates with $I_{incident}$ = 1.5 mW/cm^2. The points are experimental data, the lines are model results calculated using Eq. (20) and the fitting parameters k and K. Geometrical characteristics of R2: w = 2 mm, h = 0.5 mm and L = 70 mm.

4.1. Demonstration of mass-transfer limitation and axial dispersion

Two measurements were performed in R2 in order to characterize the axial dispersion and the mass-transfer limitation in the micro-channel reactors: residence time distribution (RTD) and comparison of the experimental degradation ratio with the Langmuir–Hinshelwood model considering a perfect plug-flow reactor. The results presented in the figures are fairly representative for the other reactors.

Fig. 7 presents RTD curves, measured at the inlet and the outlet of the reactor at different flow rates. The results are given in such a way that the area under the curve of RTD $E(t)$ is unity. The RTD curves can be described by an axial dispersion model [28], thus yielding a global reactor Peclet number Pe_R (Eqs. (4)–(6)). For flow rates of 2.5, 5 and 10 mL/h, with an effective average residence time in the reactor of 320, 95 and 40 s, respectively, Pe_R values of 23, 20 and 11 are obtained. As expected the Pe_R decreases with the flow rate. Thus, under our experimental conditions, the Pe_R yields values lower than 100, which is the commonly accepted limit for plug-flow [28]. These low values of Pe_R indicate that the reactor cannot be considered as a perfect plug-flow reactor and that significant axial dispersion occurs. The influence of the parabolic laminar velocity profile on axial dispersion is much larger than the molecular diffusion. Note also that the theoretical values of Pe (using $Pe = uL/D_a$) equal 29, 15 and 8 for flow rates of 2.5, 5 and 10 mL/h, respectively. The experimental values are close to those obtained with the calculation.

In order to demonstrate the existence of a significant mass-transfer limitation the experimental degradation ratios obtained in R2 are compared with the perfect plug-flow reactor model (Eq. (12)). In Fig. 8a, the data points for the various flow rates and inlet concentrations do not fall on a single line indicating that the micro-channel reactor cannot be simulated to a perfect plug-flow reactor. This discrepancy cannot be attributed to experimental errors. However, for a given flow rate, a linear increase of $-V/(QC_{in}X)$ as a function of $\ln(1-X)/C_{in}X$ is observed. The apparent kinetic constants (k_{app} and K_{app}) for each flow rate can be obtained using Eq. (12) from the slope and intercept point. The values of k_{app} and K_{app} are indicated in Fig. 8a. To emphasize this flow rate

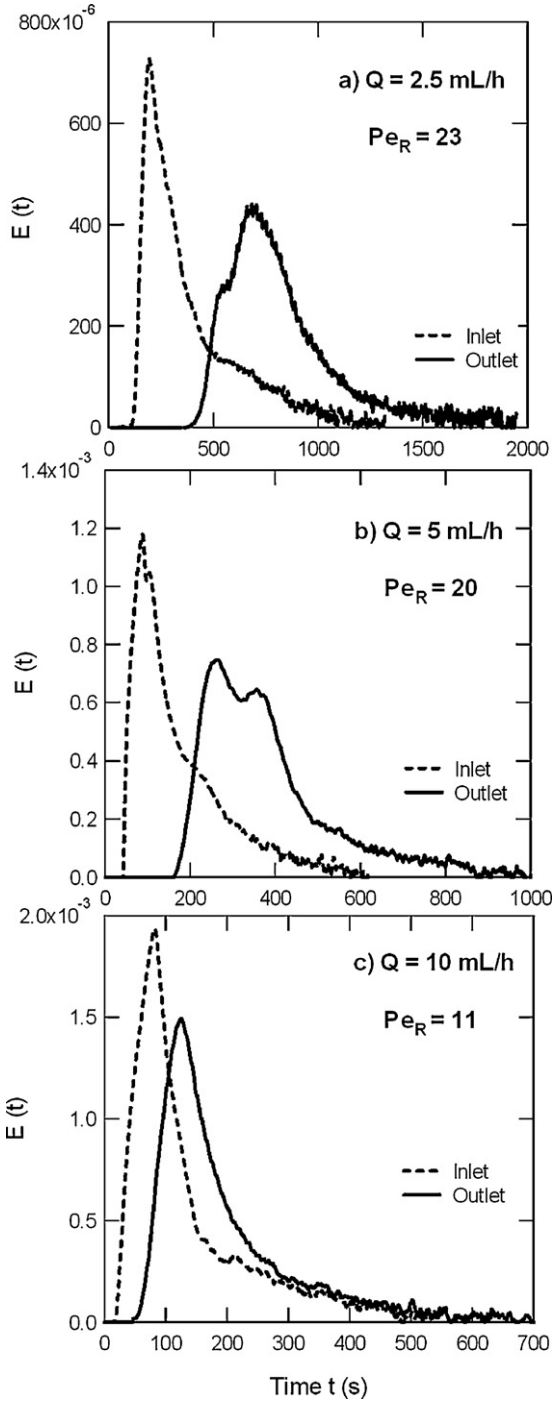

Fig. 7. Experimental residence time distribution measured at the inlet and the outlet of the micro-channel reactor R2 for three flow rates Q: (a) 2.5 mL/h, (b) 5 mL/h and (c) 10 mL/h. The experimental reactor Peclet numbers Pe_R are indicated in the figure.

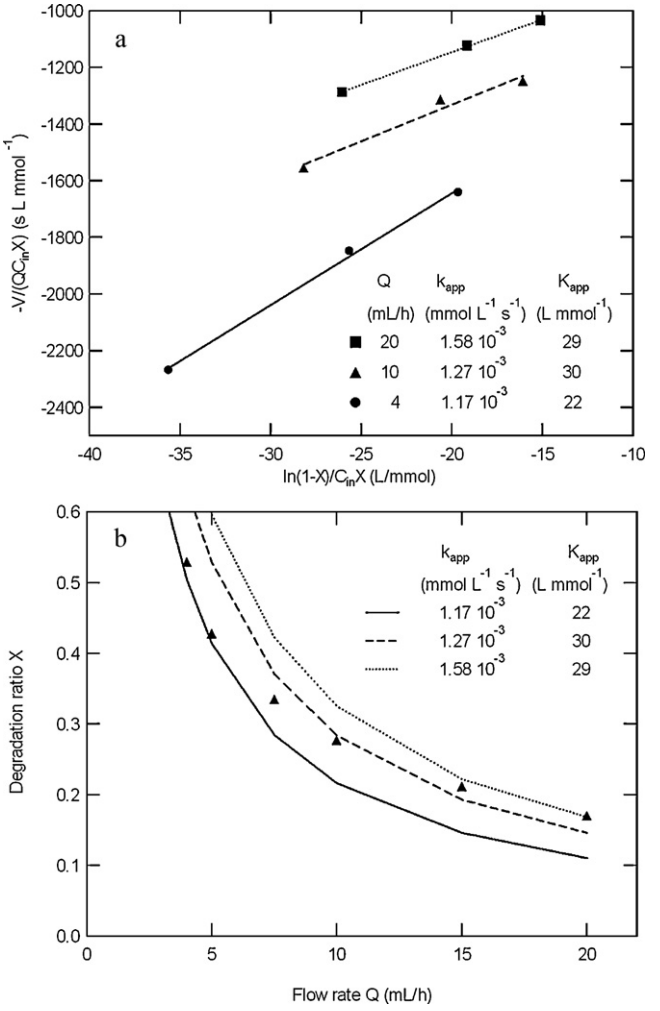

Fig. 8. Langmuir–Hinshelwood kinetics assuming a perfect plug-flow reactor. (a) Plot of $-V/(QC_{in}X)$ versus $\ln(1-X)/C_{in}X$ to test the validity of the perfect plug-flow reactor assumption in R2. The lines represent the best linear fit given by $-V/(QC_{in}X) = 23.13\ln(1-X)/C_{in}X - 682.34$ ($R^2 = 0.999$) for $Q = 20$ mL/h, $-V/(QC_{in}X) = 25.88\ln(1-X)/C_{in}X - 812.78$ ($R^2 = 0.969$) for $Q = 10$ mL/h, and $-V/(QC_{in}X) = 39.50\ln(1-X)/C_{in}X - 852.61$ ($R^2 = 0.997$) for $Q = 4$ mL/h. (b) Comparison of the experimental (symbols) and calculated (lines) degradation of salicylic acid in R2 as a function of the flow rate with $C_{in} = 10$ mg/L and $I_{incident} = 1.5$ mW/cm^2. The calculations are performed using Eq. (11) and the obtained kinetic constants k_{app} and K_{app}.

dependence, the degradation ratios are calculated, for different flow rates, using Eq. (11) and the obtained apparent kinetic constants k_{app} and K_{app}. Fig. 8b shows that a given couple of values of k_{app} and K_{app} is unable to represent the experimental degradation ratios for all the flow rates. The increase of k_{app} with the flow rate, from 1.17×10^{-3} mmol L^{-1} s^{-1} to 1.58×10^{-3} mmol L^{-1} s^{-1}, is a strong indication of a mass-transfer limitation. It is also interesting to note that k_{app} varies also significantly with the reactor dimensions (not shown). For a flow rate of 4 mL/h, k_{app} equals 1.71×10^{-3}, 1.34×10^{-3} and 1.17×10^{-3} mmol L^{-1} s^{-1} for R1, R1.5 and R2, respectively. In the same time, K_{app} corresponds to 40, 14 and 22 L mmol^{-1}. Great care has to be taken with the values of these constants. However, these values will be used for the estimation of the heterogeneous Damköhler number α which represents the ratio of the heterogeneous reaction rate at the channel walls to radial diffusion from the channel axis towards the wall (maximum possible reaction rate divided by maximum possible mass-transfer rate). For photocatalytic reactions that obey Langmuir–Hinshelwood kinetics, α is defined as [35]:

$$\alpha = \frac{k_{app}}{k_{m,ext}\kappa/K_{app} + k_{m,ext}\kappa C_{in}} \quad (24)$$

In the case where the reaction rate is limited by mass-transfer, $\alpha > 1$. For the special case of micro-channel reactors, Commenge et al. [36,37] developed a criterion which allows the estimation of the influence of mass-transfer on the kinetic measurement. They demonstrate that for α less than 0.1, the error in the measured rate constants is less than 3% and reflect the intrinsic kinetics of the investigated reaction. The calculated α are 6.7, 4.5 and 3.1 for flow rates of 4, 10 and 20 mL/h, respectively. All the α values become well

Table 2
Comparison of the values of the fitting parameters for different micro-channel dimensions ($I_{incident}$ = 1.5 mW/cm^2). k is the reaction rate constant, K the adsorption equilibrium constant, and k_a the reaction rate constant per unit coated surface ($k_a = k/\kappa$).

	K (L mmol^{-1})	k (10^{-3} mmol L^{-1} s^{-1})	k_a (10^{-4} mmol m^{-2} s^{-1})
R1	23	2.06	5.15
R1.5	25	1.68	5.04
R2	24	1.70	5.67

larger than 1. It becomes obvious that there is significant mass-transfer limitation and that the measured apparent kinetic data does not reflect the intrinsic kinetics of the photocatalytic reaction.

4.2. Determination of the kinetic constants

Eq. (20) is used to fit the experimental data using the procedure described in Section 3.3. We use k and K as fitting parameters and plot the degradation ratio as a function of the flow rate adjusting the k and K to give the best fit. We confirm the values of the kinetic constants by comparing the calculated (using Eq. (20) and the fitted kinetic constants) and the experimental degradation ratio as a function of the inlet concentration. The resulting best fits and calculated degradation ratios are shown in Figs. 4–6 for a variety of reactor dimensions, flow rates, inlet concentrations and light intensities. The values of the adjustable parameters k and K are listed in Table 2.

For a given reactor, the fit accounts for all data points (flow rates). In addition, we also obtain a good agreement between the calculated and experimental degradation ratios for all the inlet concentrations. A single couple of values of k and K represents well the experimental degradation ratios for all flow rates and inlet concentrations. The values of K and k are independent of the flow rate and the inlet concentration, which is a very strong argument in favor of the theory. This also confirms that the rate of salicylic acid decomposition follows Langmuir–Hinshelwood kinetics. The same agreement is observed for the three reactors.

The values of k and K obtained in the three reactors are compared in Table 2. The reactor dimensions do not influence the values of K which range between 23 and 25 L mmol^{-1}. The adsorption equilibrium constant only depends on the temperature and the affinity between the pollutant and the catalyst [3,23,25]. Since the experiments are performed at constant temperature with the same amount of catalyst, K is not expected to vary with the reactor geometry. The obtained values are comparable with that of about 20–25 L mmol^{-1} already reported for a similar pollutant/catalyst system [25,38]. The k values slightly vary with the reactor geometry. They range from 2.06×10^{-3} to 1.68×10^{-3} mmol L^{-1} s^{-1} which is actually within the margin of error of the kinetic constants determination. However, the k values agree with the results of Ould-Mame et al. [25] who found 3.5×10^{-3} mmol L^{-1} s^{-1} for the photocatalytic degradation of salicylic acid on fixed TiO_2 in the absence of mass-transfer limitation. The larger value of k, reported in the literature, can be explained by the higher incident light intensity (3.6 mW cm^{-2}). However, as the reaction takes place at the surface of the catalyst, it is more appropriate to express the reaction rate constant per unit coated surface k_a. k_a is obtained by normalizing k with the specific surface area κ, i.e. $k_a = k/\kappa$. Table 2 shows that k_a does not depend on the reactor geometry. As expected, the obtained reaction rate constants are independent of the reactor dimensions [6].

It is anticipated that the light intensity has a significant effect on the photocatalytic degradation rate. In order to investigate the relationship between the reaction rate constant, k, and the light intensity, $I_{incident}$, experiments were conducted at varying light intensity (Fig. 5a). The following power law, $r \propto I_{incident}^{n}$, is usually used to relate the dependence of the degradation rate to the photon flux [3,39]. According to the literature, the reaction rate increases linearly with ultraviolet intensity (n = 1) until a given intensity value around $I_{incident}$ = 25 mW cm^{-2} [3]. In R1.5, under the present experimental conditions ($I_{incident}$ from 0 to 2.8 mW cm^{-2}), it is suggested that k should be plotted as a function of $I_{incident}$. If this is done, a straight line should be obtained. In Fig. 9, a linear relationship is found experimentally (R^2 = 0.999). The dependence of the reaction rate on the incident UV intensity is first order. The reaction rate constant k is mainly determined by the incident light intensity. This confirms the photo-induced nature of the activation of the catalytic process, with the participation of photo-induced electrical charges (electrons and holes) to the reaction mechanism. This also indicates that k is a constant which only depends on the light intensity absorbed by the catalyst. In addition, it is interesting to note that the adsorption constant K does not vary with the incident intensity (see the legend in Fig. 5).

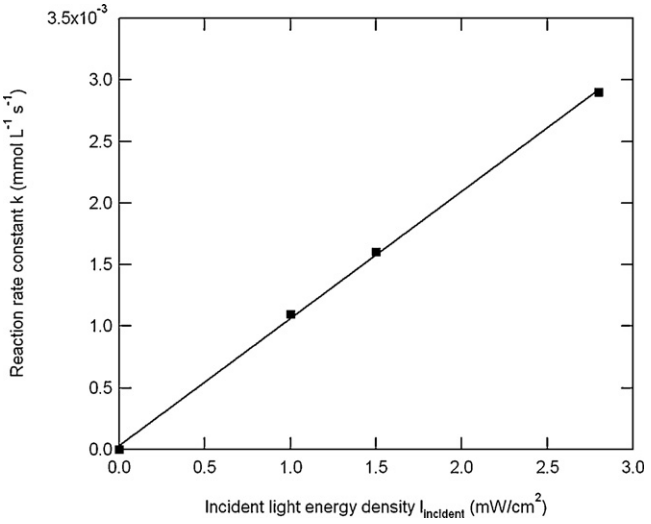

Fig. 9. Reaction rate constant versus UV incident light energy density in R1.5. The line represents the best linear fit given by $k = 0.001\ I_{incident}$ (R^2 = 0.999).

Two additional series of measurements are made to test the robustness of the model. First, experiments are performed with micro-channel reactors with different lengths. The reactors used are similar in width and height to R1 (w = 1 mm and h = 0.5 mm). In Fig. 10 the degradation ratio as a function of the channel length is reported. The degradation increases with the micro-channel length, which is explained by the increase in the residence time of the reactants in the micro-channel. We confirm the values of the kinetic constants obtained for R1 by comparing the calculated and experimental degradation ratios as a function of the micro-channel length (Fig. 10). The calculations are carried out using Eq. (20) with $k = 2.06 \times 10^{-3}$ mmol L^{-1} s^{-1} and K = 23 L mmol^{-1}. The calculated degradation ratios are in very good agreement with the experimental data for all the micro-channel lengths.

A second set of experiments is performed with the succession of the two reactors R2 and R1.5. The outlet channel of R2 is directly connected to the inlet of R1.5 to avoid dead volume and additional axial dispersion. The degradation ratio is measured at the outlet of R1.5 as a function of the flow rate (Fig. 11). The degradation decreases with the flow rate. As expected, the degradation performance is strongly affected by the number of micro-channels. The degradation is significantly higher for the two reactors configuration. A degradation ratio of 0.8 is obtained for a flow rate of 3 mL/h which is the highest degradation ratio obtained in the present study. The values of the kinetic constants are checked by comparing the calculated and

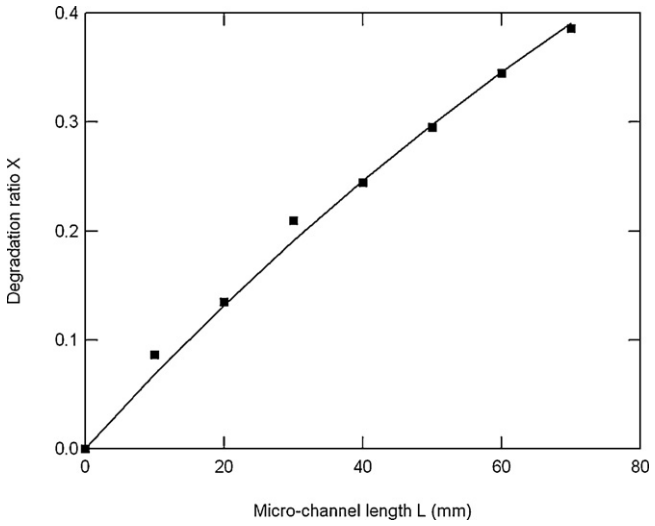

Fig. 10. Degradation of salicylic acid as a function of the micro-channel length with C_{in} = 10 mg/L, Q = 5 mL/h and $I_{incident}$ = 1.5 mW/cm^2. The reactors used are similar in width and height to R1 (w = 1 mm and h = 0.5 mm). Comparison of the experimental (symbols) and calculated (line) degradation curves. The calculations are performed using Eq. (20) and $k = 2.06 \times 10^{-3}$ mmol L^{-1} s^{-1}, K = 23 L mmol^{-1}.

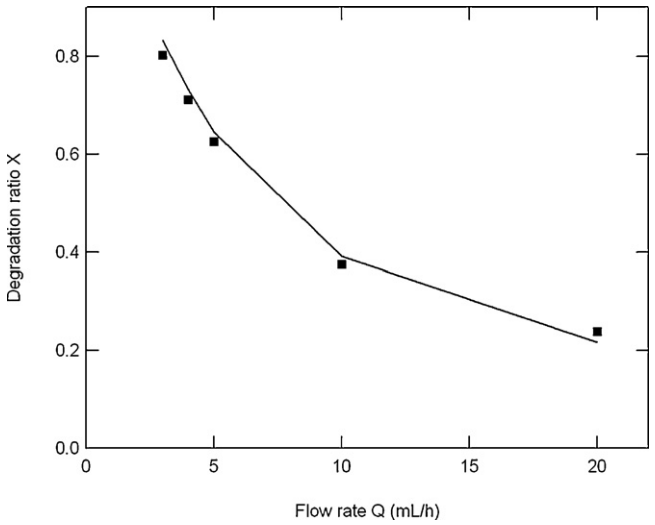

Fig. 11. Degradation of salicylic acid at the outlet of the series of the two micro-channel reactors R2 and R1.5 as a function of the flow rate with C_{in} = 10 mg/L and $I_{incident}$ = 1.5 mW/cm^2. The outlet of reactor R2 is directly connected to the inlet of reactor R1.5. Comparison of the experimental (symbols) and calculated (line) degradation curves.

experimental degradation ratios. The calculations are carried out using a stepwise procedure. First, the outlet concentration from the reactor R2 (C_{out}(R2)) is estimated with Eq. (19). The parameters used in calculations are $k = 1.70 \times 10^{-3}$ mmol L^{-1} s^{-1} and K = 24 L mmol^{-1}. Then, the outlet concentration (C_{out}(R2 + R1.5)) from the second reactor is obtained using C_{out}(R2) as the inlet concentration, $k = 1.68 \times 10^{-3}$ mmol L^{-1} s^{-1} and K = 25 L mmol^{-1}. It is then possible to evaluate the degradation ratio, given here as $X = 1 - C_{out}(R2 + R1.5)/C_{in}(R2)$. In Fig. 11 the calculated degradation ratio is plotted against the flow rate (line). A very good agreement between the calculated and experimental data is still observed.

5. Conclusions

The aim of this paper was to determine the kinetic constants during the photocatalytic degradation of salicylic acid in micro-channel reactors despite the presence of radial concentration profile (mass-transfer limitation) and axial dispersion.

Photocatalytic micro-channel reactors with immobilized titanium dioxide as photocatalyst have been designed, constructed and tested. The micro-channel reactors are fabricated using stereolithography and the surface of the channel is coated using an aqueous suspension of TiO_2. The photocatalytic degradation of salicylic acid is investigated as a function of rectangular micro-channel size, contaminant concentration, flow rate and incident light intensity. All the micro-channel reactors show the same tendency. Higher degradation ratio is observed for high incident light intensities, low pollutant concentrations and flow rates.

A simple equation for the determination of the kinetic constants during the photocatalytic degradation of salicylic acid in the micro-channel reactors is presented. The equation employs the hydrodynamic properties and a surface reaction model for the photocatalytic reaction. The equation considers that the reaction rate can be modeled by a monomolecular Langmuir–Hinshelwood law. The external mass-transfer limitation and axial dispersion are included in the modeling with calculated values of the mass-transfer coefficient $k_{m,ext}$ and the axial dispersion coefficient D_a. For an incident light intensity of 1.5 mW cm^{-2}, a single couple of values of k and K represent properly the experimental degradation ratios for all the reactor dimensions, flow rates and inlet concentrations. The obtained values for the adsorption equilibrium constant K and the reaction rate constant k are $K = 24 \pm 1$ L mmol^{-1} and $k = 1.81 \times 10^{-3} \pm 0.21 \times 10^{-3}$ mmol L^{-1} s^{-1}. The reaction rate constant k is significantly affected by the incident light intensity. The dependence of the reaction rate on the incident UV intensity is first order.

It is clear that, despite its simplicity, the model captures the essential physics of the photocatalytic degradation of salicylic acid for the determination of the kinetic constants without recourse to numerical simulations (CFD). Both the radial concentration profile and the axial dispersion are well described. We report a simple and rapid approach for the accurate determination of the kinetic constants during a photocatalytic reaction. This general methodology can be used for the determination of the kinetic constants for any reactor design and any organic pollutant, regardless of the immobilized photocatalyst nature. This work also indicates the potentiality of micro-channel reactors for the determination of the activity of the photocatalyst avoiding the fabrication of several, time consuming and highly costing, reactor prototypes.

Acknowledgement

This work was financially supported by grants of the “Region de Lorraine”.

References

[1] M.R. Hoffmann, S.T. Martin, W. Choi, D.W. Bahnemann, Chem. Rev. 95 (1995) 69–96.
[2] D. Bahnemann, Photocatalytic detoxification of polluted waters, in: Environmental Photochemistry, Springer-Verlag, Berlin, 1999.
[3] J.M. Herrmann, Appl. Catal. B: Environ. 99 (2010) 461–468.
[4] P.S.M. Dunlop, J.A. Byrne, N. Manga, B.R. Eggins, J. Photochem. Photobiol. A 148 (2002) 355–363.
[5] A. Mills, G. Hill, S. Bhopal, I.P. Parkin, S.A. O'Neil, J. Photochem. Photobiol. A 160 (2003) 185–194.
[6] M.F.J. Dijkstra, H.J. Panneman, J.G.M. Winkelman, J.J. Kelly, A.A.C.M. Beenackers, Chem. Eng. Sci. 57 (2002) 4895–4907.
[7] A.K. Ray, A.A.C.M. Beenackers, AIChE J. 44 (1998) 477–483.
[8] S. Ahmed, C.E. Jones, T.J. Kemp, P.R. Unwin, Phys. Chem. Chem. Phys. 1 (1999) 5229–5233.
[9] D.F. Ollis, E. Pelizzetti, N. Serpone, Environ. Sci. Technol. 25 (1991) 1522–1529.
[10] M.F.J. Dijkstra, H. Buwalda, A.W.F. de Jong, A. Michorius, J.G.M. Winkelman, A.A.C.M. Beenackers, Chem. Eng. Sci. 56 (2001) 547–555.
[11] R. Gorges, S. Meyer, G. Kreisel, J. Photochem. Photobiol. A: Chem. 167 (2004) 95–99.

[12] B.C. Choi, L.H. Xu, H.T. Kim, D.W. Bahnemann, J. Ind. Eng. Chem. 12 (2006) 663–672.
[13] T. Van Gerven, G. Mul, J. Moulijn, A. Stankiewicz, Chem. Eng. Process. 46 (2007) 781–789.
[14] S. Teekateerawej, J. Nishino, Y. Nosaka, J. Photochem. Photobiol. A: Chem. 179 (2006) 263–268.
[15] D.G. Shchukin, D.V. Sviridov, J. Photochem. Photobiol. A 7 (2006) 23–39.
[16] D.H. Chen, X. Ye, K. Li, Chem. Eng. Technol. 28 (2005) 95–97.
[17] A. Queffeulou, L. Geron, C. Archambeau, H. Le Gall, P.M. Marquaire, O. Zahraa, Ind. Eng. Chem. Res. 49 (2010) 6890–6897.
[18] M. Mohseni, F. Taghipour, Chem. Eng. Sci. 59 (2004) 1601–1609.
[19] I. Salvado-Estivill, D.M. Hargreaves, G. Li Puma, Environ. Sci. Technol. 41 (2007) 2028–2035.
[20] A. Queffeulou, L. Geron, E. Schaer, Chem. Eng. Sci. 65 (2010) 5067–5074.
[21] M. Furman, S. Corbel, H. Le Gall, O. Zahraa, M. Bouchy, Chem. Eng. Sci. 62 (2007) 5312–5316.
[22] T. Roques-Carmes, P. Marchal, A. Gigante, S. Corbel, Russ. Chem. Rev. 78 (2009) 375–386.
[23] M. Furman, S. Corbel, G. Wild, O. Zahraa, Chem. Eng. Process. 49 (2010) 35–41.
[24] G. Charles, S. Corbel, M.C. Carre, T. Roques-Carmes, O. Zahraa, Proc. 4th International Conference on Innovative Developments in Design and Manufacturing, 2010, pp. 431–434.
[25] S.M. Ould-Mame, O. Zahraa, M. Bouchy, Int. J. Photoenergy 2 (2000) 59–66.
[26] J.M. Commenge, T. Obein, G. Genin, X. Framboisier, S. Rode, V. Schanen, P. Pitiot, M. Matlosz, Chem. Eng. Sci. 61 (2006) 597–604.
[27] M. Günther, S. Schneider, J. Wagner, R. Gorges, T. Henkel, M. Kielpinski, J. Albert, R. Bierbaum, J.M. Köhler, Chem. Eng. Sci. 101 (2004) 373–378.
[28] O. Levenspiel, Chemical Reaction Engineering, 3rd ed., John Wiley & Sons, New York, 1999.
[29] D.F. Ollis, E. Pelizzetti, N. Serpone, Photocatalysis—Fundamentals and Applications, Wiley, New York, 1989.
[30] M. Bouchy, O. Zahraa, Int. J. Photoenergy 5 (2003) 191–197.
[31] M. Polakovic, T. Gorner, F. Villiéras, P. de Donato, J.L. Bersillon, Langmuir 21 (2005) 2988–2996.
[32] J.M.P.Q. Delgado, J. Phase Equilibr. Diffusion 28 (2007) 427–432.
[33] O. Barlay Ergu, O.N. Sara, S. Yapici, M.E. Arzutug, Int. Commun. Heat Mass-transfer 36 (2009) 618–623.
[34] E. Guinea, C. Arias, P.L. Cabot, J.A. Garrido, R.M. Rodriguez, F. Centellas, E. Brillas, Water Res. 42 (2008) 499–511.
[35] D.D. Dionysiou, M.T. Suidan, I. Baudin, J.M. Laîné, Appl. Catal. B: Environ. 38 (2002) 1–16.
[36] J.M. Commenge, L. Falk, J.P. Corriou, M. Matlosz, Proc. 5th International Conference on Microreaction Technology, Springer, Berlin, 2002, pp. 131–140.
[37] J.M. Commenge, Ph.D. Thesis, University of Nancy, France, 2001.
[38] A. Mills, C.E. Holland, R.H. Davies, D. Worsley, J. Photochem. Photobiol. A: Chem. 83 (1994) 257–263.
[39] S. Brosillon, L. Lhomme, C. Vallet, A. Bouzaza, D. Wolbert, Appl. Catal. B: Environ. 78 (2008) 232–241.